ORIGINAL PAPER

Response of landslide deformation to rainfall based on multi-index monitoring: a case of the Tanjiawan landslide in the Three Gorges Reservoir

Li Wang[1,2] · Yushan Chen[1,2] · Shimei Wang[1,2] · Fei Guo[1,2]

Abstract

Landslide deformation in the Three Gorges Reservoir Area (TGRA) is mainly caused by water level fluctuations; however, it is also influenced by rainfall. The Tanjiawanlandslide is one of the most notable landslides affected by rainfall in the TGRA. This study investigates the landslide's deformation mechanism by analysing reconnaissance data, which are surface deformation survey data, and GPS displacement data for the last 16 years along with several types of monitoring data from equipment installed in 2020. The landslide has undergone significant deformation since September 2014. Subsequent rainfall events have caused severe deformation, and tension cracks have appeared in many parts of the landslide. Owing to the slope structure and rainfall events, a deformation feature has developed, in which sliding masses no. 1 and no. 2 are the active and secondary deformation zones, respectively. The surface displacement of the landslide is clearly step-like, and its episodic deformation is controlled by rainfall. Landslide deformation leads to the development of cracks in the slope, producing dominant seepage channels. As rainwater enters belowground along the cracks and with the influence of the bedrock morphology, the groundwater level in the middle and rear parts, and hence, the hydrodynamic pressure, increase, thereby activating landslide deformation. Both continuous rainfall and heavy rain are responsible for this phenomenon; sliding mass no. 1 shows an overall downward motion. Finally, the seismic data recorded by microcore piles and the change rate in soil moisture content after rainfalls can currently be used for reliable early warnings of landslide instability.

Keywords Three Gorges Reservoir · Rainfall-induced landslide · Monitoring system · Deformation mechanism

Introduction

Geological hazards in China, especially in the Three Gorges Reservoir Area (TGRA), manifest themselves primarily in the form of landslides. Since the impoundment of the Three Gorges Reservoir (TGR), a 660-km-long reservoir bank has been formed (Wang et al. 2014), and more than 5000 landslides have been identified (Huang et al. 2020a, b). Owing to long-term fluctuations in the reservoir water level, 151 landslides have undergone significant deformation; among these,

14 landslides showing a cumulative deformation exceeding 1000 mm have caused great concern, for example, the Shuping landslide (Wang et al. 2008; Wu et al. 2019) and the Bazimen landslide (Du et al. 2013; Zhou et al. 2016). In addition to the influence of reservoir water level fluctuation, rainfall is another important factor that has induced landslide deformation in the TGRA (Tang et al. 2019), as this area experiences heavy rainfall. Over time, rainfall has resulted in numerous landslide deformations and slides. For example, extremely heavy rain in July 1982 triggered the reactivation of the Jipazi landslide (volume 15 million m^3; Ding et al. 2006). The torrential rain on 31 August 2014 caused 1014 landslides in Northeastern Chongqing in the TGRA, and in 2017, prolonged autumn rain in West China caused hundreds of landslides in the Hubei section. Multiple rainfall events in June and July 2020 caused some landslides in the TGRA to deform, including the Shaziba landslide on Qingjiang River in Enshi, Hubei, with a volume of 15 million m^3 (Song et al. 2020). These events demonstrate that rainfall is a highly potent factor causing landslides in the

✉ Shimei Wang
shimeiwang1965@126.com

1 Key Laboratory of Geological Hazards On Three Gorges Reservoir Area, Ministry of Education, China Three Gorges University, Yichang 443002, Hubei, China

2 National Field Observation and Research Station of Landslides in Three Gorges Reservoir Area of Yangtze River, China Three Gorges University, Yichang 443002, Hubei, China

TGRA, and a response relationship between rainfall and landslide deformation is a key issue that needs to be investigated for effective landslide prevention and management.

Currently, there are two commonly used methods for studying the mechanism of rainfall-induced landslides. One is based on the theory of unsaturated seepage and uses numerical methods to simulate slope rainfall infiltration, which affects stability (Alonso et al. 1995; Damiano 2019). However, owing to the complexity of the rock–soil slope structure, relevant theories based on numerical simulation methods that can reveal the deformation mechanism of landslides require further development. The other method is physical model testing, which is effective in identifying the deformation characteristics and mechanisms of landslides. Hojat et al. (2019) performed a rainfall-triggered landslide model test and found that critical soil saturation, rainfall intensity, and rainfall duration (Lora et al. 2016; Wu et al. 2020) are the most important factors affecting slope stability. A more reliable method is the field model test (Rahardjo et al. 2005; Sun et al. 2019; Wang et al. 2021a, b); however, this test is typically implemented on very small shallow slopes, which is a limitation in determining the deformation mechanism of large-scale landslides. Studies on large-scale landslides using multiple monitoring methods can effectively compensate for the shortcomings of the field tests. Among these methods, the on-site hydrological monitoring of landslide soil, such as monitoring volumetric water content (Baum and Godt 2010; Dikshit and Satyam 2019) and real-time saturation monitoring (Mirus et al. 2018), is a very effective means for predicting the occurrence of landslides, especially for shallow sliding (Godt et al. 2008). However, as a hydrological monitoring indicator, soil water content can only reflect conditions that can lead to shallow landslide triggering, without accurately predicting the failure mechanism. More effective results may be obtained based on water content monitoring combined with pore water pressure monitoring (Bordoni et al. 2015, 2021). Therefore, the combination of hydrological and landslide deformation monitoring is an important means to investigate the mechanism of landslide occurrence. Many researchers have used monitoring data to examine the rainfall response of large-scale landslides in the TGRA (Tang et al. 2015; Liu et al. 2018; Huang et al. 2020a, b). These studies are of great significance for landslide early warnings and understanding the rainfall trigger mechanism of landslides. With the continuous development of landslide monitoring technology, current landslide deformation and hydrological monitoring include high-precision and real-time monitoring; this will provide important support for the prevention and mitigation of landslides.

The Tanjiawan landslide is a typical rainfall-induced landslide in the TGRA. It exhibited large deformation responses to all three of the recent extreme rainfall events in the TGRA mentioned above. Therefore, this study took the Tanjiawan landslide as the research object, using surface deformation surveys, surface crack data, and GPS displacement data for the past 16 years to analyse the characteristics of rainfall-induced deformations. To further examine the influence of different rainfall events on the Tanjiawan landslide, a series of new monitoring technologies were applied to the Tanjiawan landslide after January 2020, including global navigation satellite system (GNSS) surface displacement, deep displacement, soil moisture content, and groundwater level data. The research results can aid in the prevention of landslides triggered by rainfall in the TGRA. By analysing the response relationship between the monitoring data and rainfall, an attempt was made to reveal the deformation mechanism of the Tanjiawan landslide.

Overview of the Tanjiawan landslide

Morphological characteristics of the landslide

The Tanjiawan landslide is located on the right bank of the Zhaxi River, a tributary of the Yangtze River, in the TGRA. It is 10.8 km from the river's entrance into the Yangtze River in Shangba Village, Shuitianba Township, Zigui County (Fig. 1). The middle of the landslide is concave, the elevation of the trailing edge of the landslide reaches 370–380 m, and there is a bedrock outcropping outside the boundary of the trailing edge of the landslide, with a rock occurrence of $30° \angle 12°$. The leading edge of the landslide reaches the Zhaxi River. The elevation in the middle of the landslide and south of the leading edge is 168–170 m, and the elevation in the north is 200 m. The right side of the landslide is bounded by a gully with a width and depth of 1–5 and 2–4 m, respectively. The left boundary is a small mountain beam (Fig. 2). The slope of the landslide is 25°–35°, and the longitudinal section of the landslide is in the shape of a broken line. The maximum longitudinal length of the sliding mass is 440 m, and the transverse width is 210–250 m (Fig. 3). The thickness of the sliding mass is uneven; the thickness at the rear of the landslide is approximately 17–34 m, the thickness at the front is approximately 6–17 m, and the thickness of the middle is decreased owing to the convex influence of the bedrock. The total volume is approximately 282.5×104 m^3. Over the years, the main sliding direction has been 68° from North. Based on its characteristics, the deformation area of the Tanjiawan landslide can be divided into sliding masses no. 1 and no. 2 (Fig. 2); the former is the main deformation area (Fig. 3).

Landslide geological conditions

Zigui County, where the landslide is located, is in a subtropical continental monsoon climate zone, with a mild
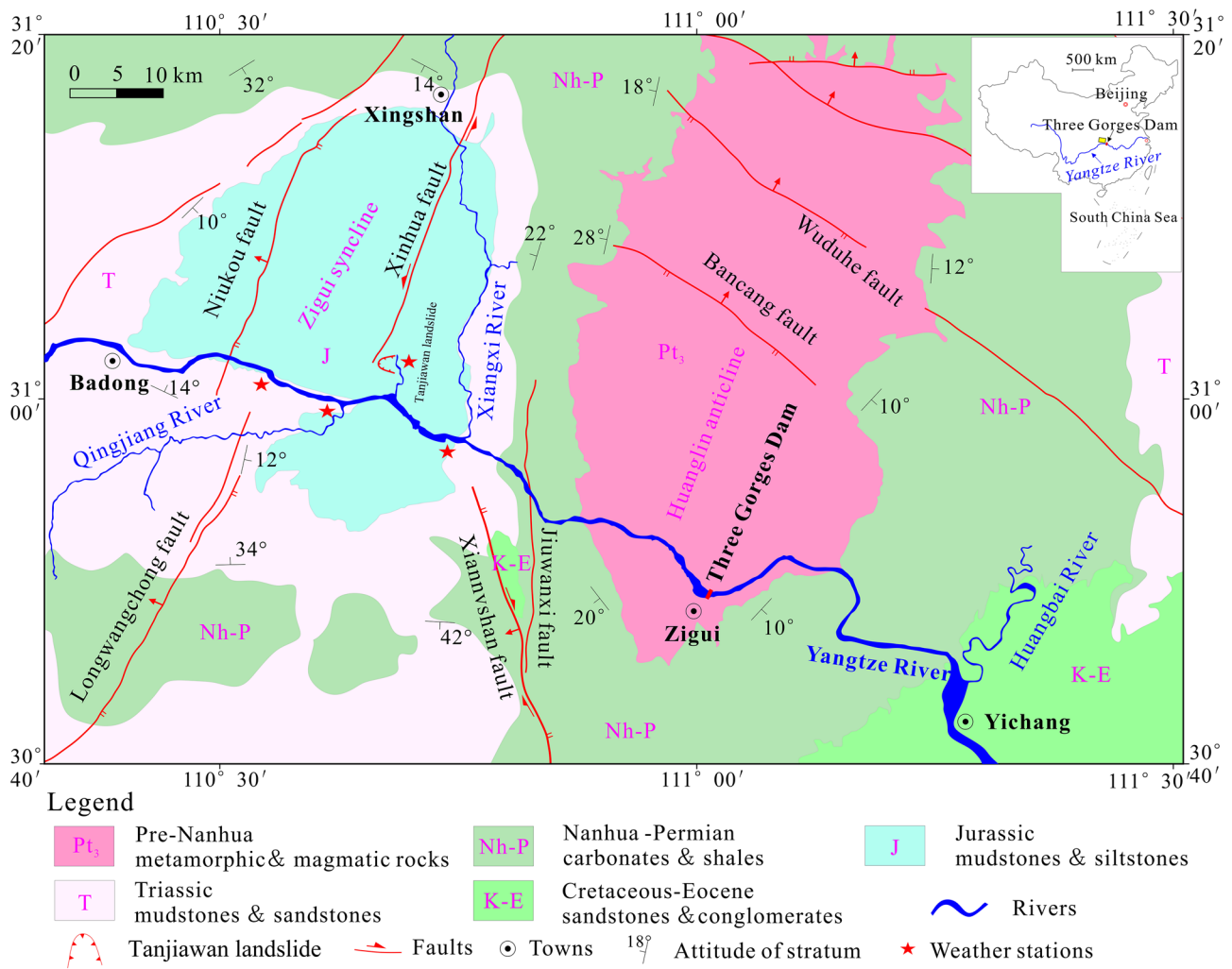
Fig. 1 Geographic location of the landslide and lithology distribution map of the stratum

and humid climate, abundant rainfall, and four distinct seasons. The average annual temperature in the area is 17–19 °C, and the average annual rainfall is 1493.2 mm. The character of the rainfall is continuous and concentrated, with heavy rains during the rainy season and a maximum daily rainfall of 358 mm. Generally, the annual rainfall is 950–1590 mm and approximately 1000 mm in the Yangtze River valley. Rainfall is mainly concentrated during April–October, with an average monthly rainfall of 150–457.6 mm, and heavy rains with daily rainfalls of 50–100 mm occur from April to October. According to the statistical results of historical rainfall data provided by *Institute of Heavy Rain, China Meteorological Administration* (*Wuhan*), heavy rains above 100 mm mainly occur in June and July, with an average annual frequency 3–4 times, the results of the field investigation showed that this is also the main hydrodynamic factor for the strong deformation of the Tanjiawan landslide.

The main structural trace in the area is the Zigui syncline, which has an axially S-shaped open symmetry that runs nearly north–south, turning to a near east–west direction on the south side of the Yangtze River. The inclination angle of the S(E) wing is more than 30° and that of the N(W) wing is 16–30°. The core stratum is the upper Jurassic Penglai Formation, with an axial length of 47 km. As shown in Fig. 1, the landslide area is located at the core of the Zigui syncline, the nearby folds and faults are not developed, and the rock formations generally tend to be in the northeast area. Affected by the regional structure, the north-northeast and near east–west fractures in the quartz sandstone are relatively developed. Furthermore, the landslide bedrock also includes weak mudstone, and the interlaced soft and hard rock layers are the lithological conditions for the formation of the landslide.

Owing to the continuous deformation of the Tanjiawan landslide and the risk of instability, the management department

Fig. 2 Panoramic view of the Tanjiawan landslide
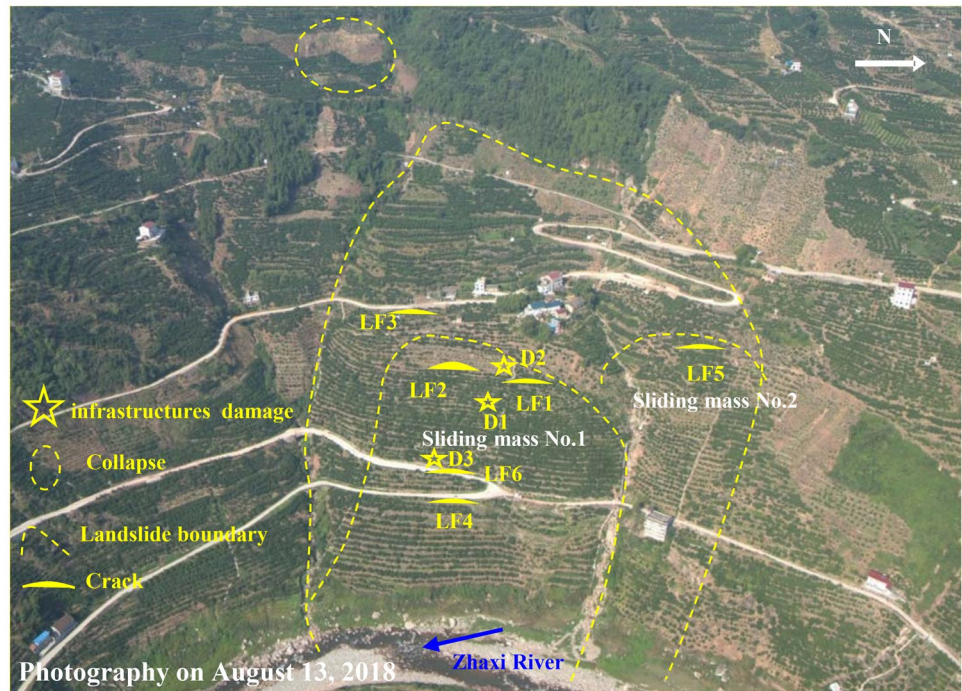
organised and completed a geotechnical engineering investigation of the landslide in 2019, and three main profiles were described. Engineering geological profiles 1–1′ and 2–2′ on sliding mass no. 1 in the main deformation area were based on the results of a geophysical exploration and drilling (Fig. 4). As evident from the figure, the two main profiles indicate two regions in the longitudinal direction. The upper half of the profile has an overall arc shape, whereas the rupture surface at the back edge is steep, and the middle part is convex. The lower half is linear in shape with a slightly steeper front; the sliding mass at the back of the landslide is thick, whereas the sliding mass at the leading edge is thin. The sliding mass in the middle is thinner owing to the presence of a convex bedrock portion, which also immobilises the upper sliding mass to some extent.

According to the investigation results, the sliding mass of the Tanjiawan landslide is mainly composed of gravel siltstone, which is yellowish-reddish brown. The thickness of the sliding mass is distributed unevenly between the two gullies and is affected by the convex bedrock surface in the middle of the landslide; thus, it is thick at both ends and thin in the middle. The slide surface soil is mainly gravelly silty clay (Fig. 4a, b), which is reddish brown or brownish yellow in colour. The thickness of the slide belt is approximately 0.2–0.4 m, and the average thickness is 0.3 m. The slide belt is located in the contact position of rock and soil; the lower part is interbedded with magenta argillaceous siltstone and quartz sandstone and is relatively impervious. The strength of the slide surface soil is low, and the slide surface soil has not been fully penetrated.

The bedrock is composed of quartz sandstone and purplish-red sandstone-mudstone of the upper Jurassic Penglai Formation. A drilling core is shown in Fig. 4b. It has a soft, sandy structure with thick strata and belongs to the engineering geological group of soft and relatively hard stratified argillaceous sandstone; its mechanical strength is not uniform. According to the exploration data, the purplish-red argillaceous siltstone is fragile when hammered and cracks easily along the layers. Monoclinic structures are present in the area. The bedrock dip angle is 12–15°, and thus, a slope is formed. No fracture zone was found in the exploration area. The photos of the soil samples of the sliding mass soil and the sliding surface soil are shown in Fig. 4a, b. The physical and mechanical parameters and permeability of the landslide soil were determined by field and laboratory tests; the properties of these soil samples are tested in accordance with China geotechnical engineering test code (SL237-1999 1999). Table 1 shows the physical and mechanical parameters of the sliding mass and sliding surface soils.

The permeability of clay is a key parameter affecting rainfall infiltration (Fig. 5). Therefore, six pit seepage tests were performed in the field, with a test depth of 0.5 m. The permeability coefficient of the surface gravel in the sliding mass soil was in the range of 1.7×10^{-4}–7.7×10^{-3} cm/s, and the sliding mass is characterised by high permeability in the middle part and low permeability in the rear part of the landslide. In addition, saturated permeability tests of the borehole sliding mass soil from different depths were
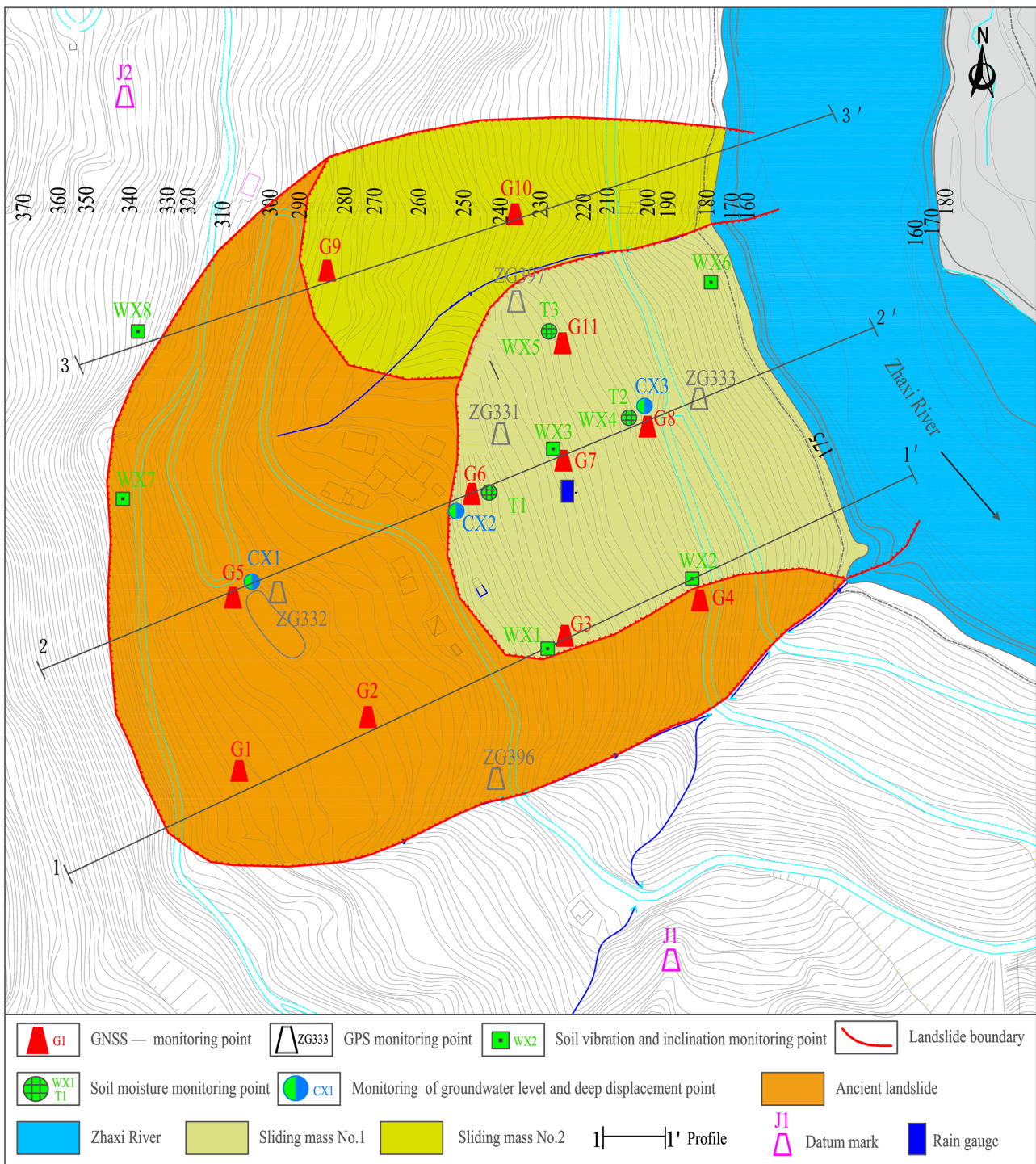
**Fig. 3** Planar and monitoring setup map of the Tanjiawan landslide

performed in the laboratory; the permeability coefficient of the sliding mass soil decreased with increasing depth and was distributed between 5×10^{-5} and 0.5×10^{-5} cm/s, which indicated weak permeability.

Landslide activity features

Since 2006, monthly surface deformation monitoring of the Tanjiawan landslide has been conducted. The results
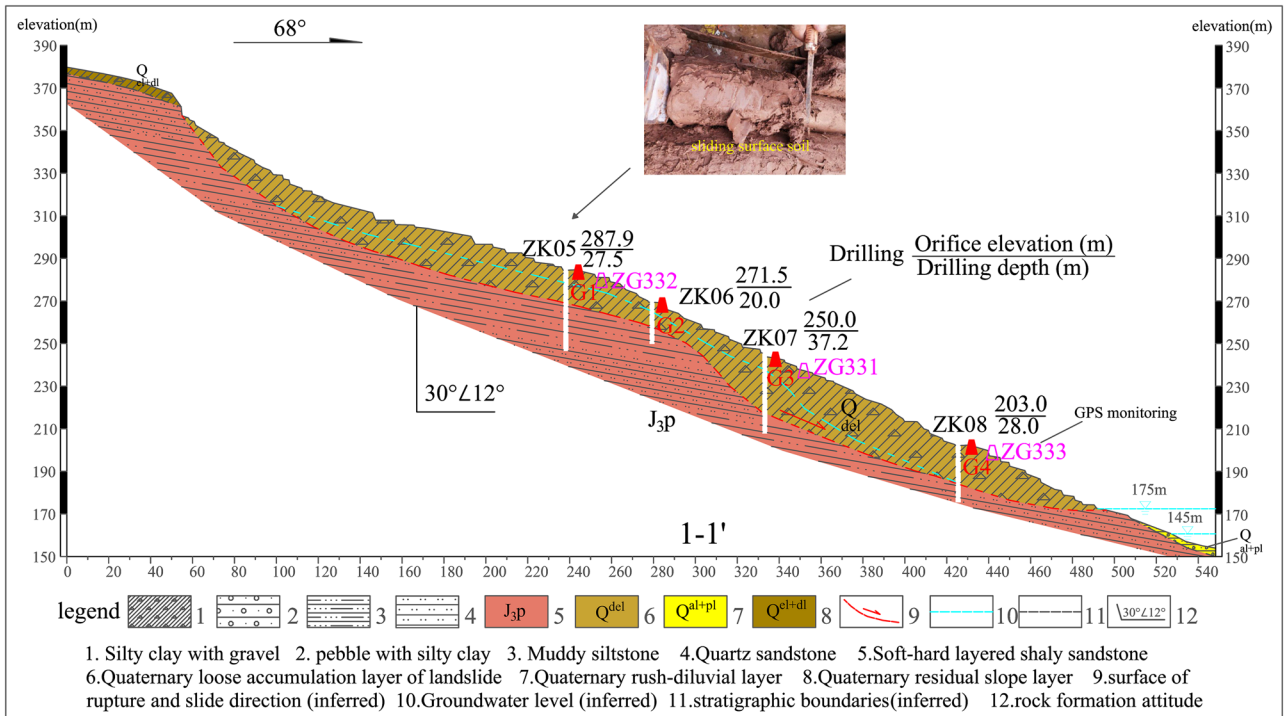
(a)
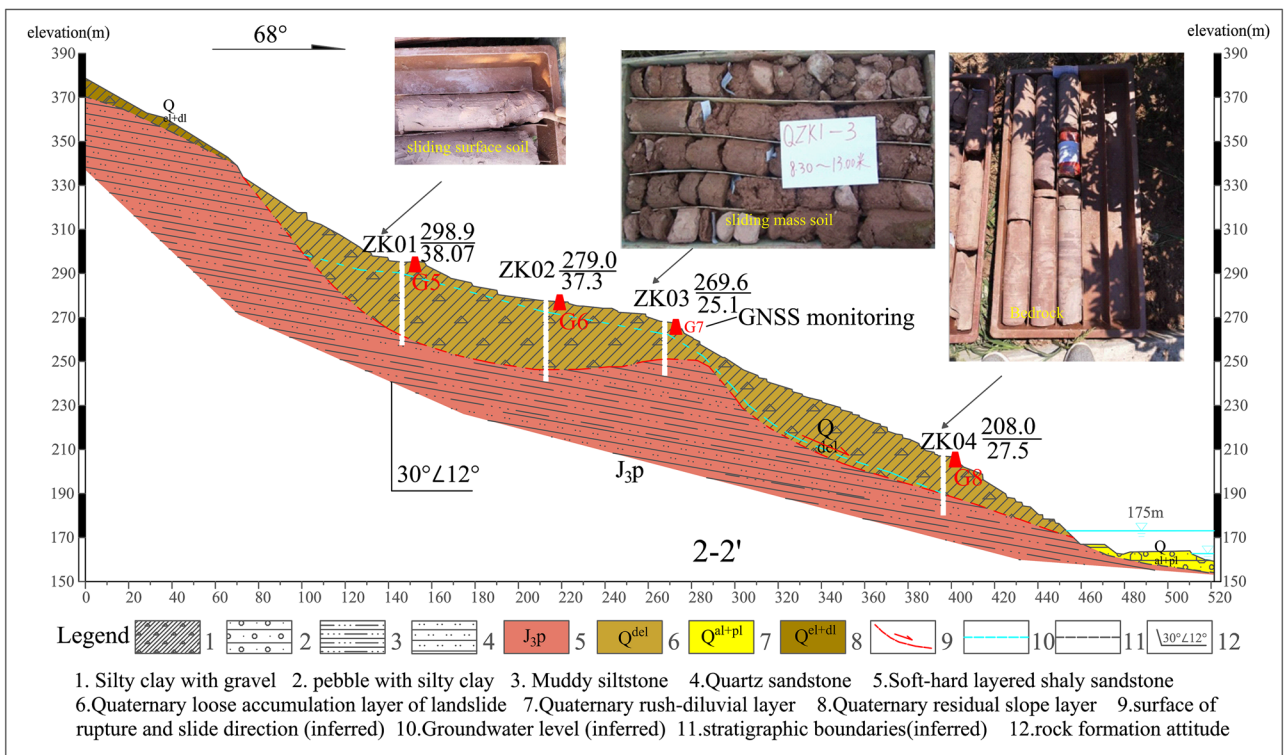
(b)

Fig. 4 Engineering geological profile: **a** geological cross Sect. 1–1′, **b** geological cross Sect. 2–2′

Table 1 Basic physical and mechanical parameters of the Tanjiawan landslide soil

Soil type	Specific gravity	Density (g/cm^3)	Dry density (g/cm^3)	Void ratio	Plasticity index	Liquidity index	Liquid limit (%)	Cohesion (kPa)	Internal friction angle (°)
Sliding mass	2.73	2.04	1.74	0.57	14.70	0.02	29.38	41.30	18.30
Sliding surface	2.73	2.04	1.72	0.56	13.65	0.02	33.22	48.6	18.6

indicate that the macro-deformation of the landslide is characterised by stages and is closely related to the annual rainfall. The main deformation process is as follows.

Prior to 2014, the surface deformation characteristics of the landslide were not obvious, and only the middle part of the landslide exhibited slight creep deformation. During the rainstorm of 31 August 2014 (mentioned in "Introduction"), three rainstorms produced a total rainfall of 270 mm in 5 days, and the Tanjiawan landslide exhibited obvious deformation and collapse. The deformation occurred as follows. The trailing edge of the landslide, with a volume of approximately 1000 m^3, collapsed (Fig. 6a), which damaged the highway (Fig. 6b). The location of the damage is shown in Fig. 2. The middle part of the landslide, with a height of approximately 30 cm, collapsed (Fig. 6c). Two tension cracks (Fig. 6d) approximately 30 m and 8 m in length are visible at the collapse site; the cracks (LF1, Fig. 2) are almost parallel, with a trend of approximately 150°.

In October 2017, owing to the effects of the autumn rain in West China, various degrees of deformation occurred in the front, middle, and back parts of the Tanjiawan landslide. Cracks appeared in the middle and back parts, causing houses to collapse (Fig. 7a). The cracks (LF2; Fig. 2) extended to the left gully; they were approximately 80 m in

length, 1–10 cm in width, and showed a maximum dislocation of 30 cm (Fig. 7b). Cracks appeared at the bottom of the retaining wall along the farm track in the middle of the landslide (Fig. 7c, the location is shown in D1 in Fig. 2), and cement steps were damaged (Fig. 7d, the location is shown in D2 in Fig. 2).

The daily rainfall in the landslide area was 121.6 mm on 18 June 2018 and 27.4 mm on 30 June 2018. Owing to these two rainfall events, the surface of the middle of the landslide exhibited obvious deformation, the main manifestations of which were as follows. The lateral crack in the highway in the middle and at the back of the landslide (Fig. 8a) was approximately 50 m long and 2–15 cm wide and was lowered by 5–25 cm (LF3; Fig. 2). The highway retaining wall in the middle and front parts of the landslide bulged (Fig. 8b) and cracked (LF4; Fig. 2). According to the deformation characteristics of the landslide, the main deformation area was labelled sliding mass no. 1, and the area with relatively weak deformation was labelled sliding mass no. 2, as shown in Figs. 2 and 3.

Multiple strong rains occurred in the landslide area from 23 to 28 June 2020; the cumulative rainfall was 199.8 mm. On 2 July 2020, the rainfall amount was 42 mm. These rainfall events caused the sliding masses no. 1 and no. 2 to be
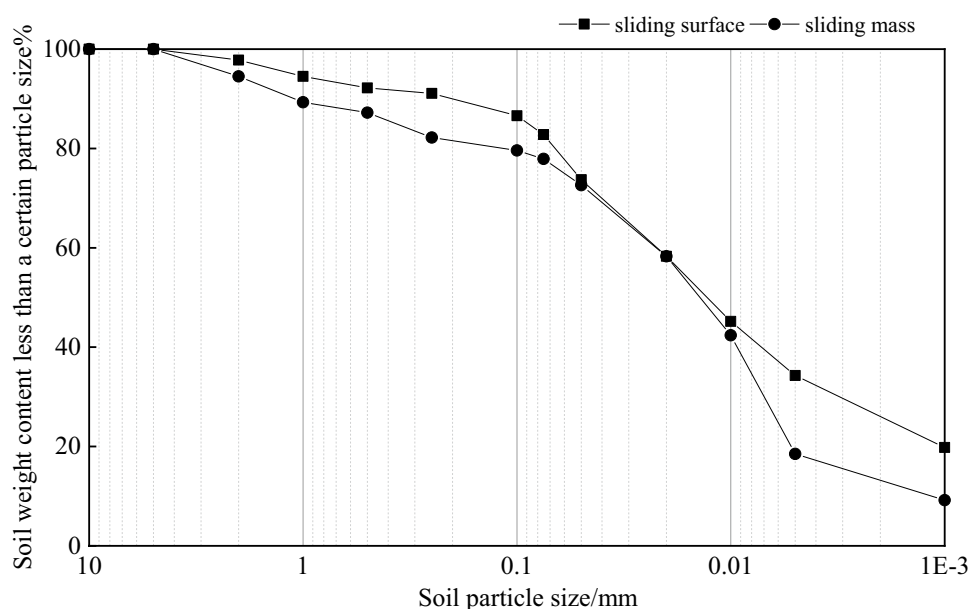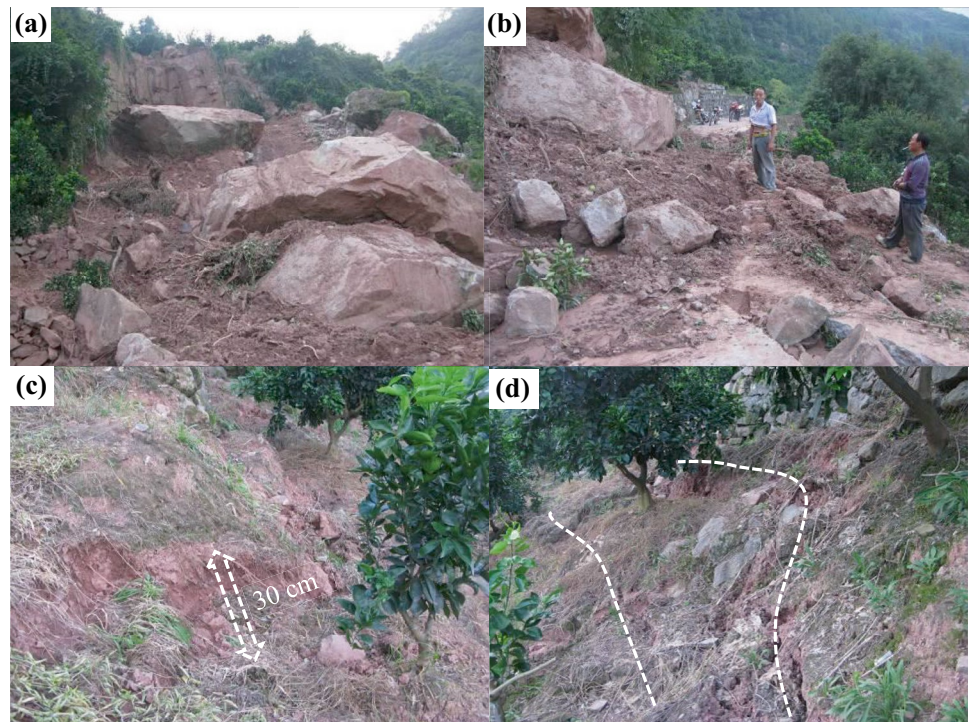
Fig. 5 Grain size distribution curve

Fig. 6 Deformation of the Tanjiawan landslide after the rainfall on 31 August 2014: **a** large-scale collapse at the back edge of the landslide, **b** resulting damage to the road behind the landslide, **c** collapse in the middle of the landslide, **d** crack LF1 in the middle of the landslide

greatly deformed. Specifically, the crack deformation in the middle of the landslide intensified, resulting in a small-scale failure of the retaining wall (Fig. 9a). This deformation was a further extension of the original deformation (Fig. 7c). The back of sliding mass no. 1 was deformed, forming a deep crack (LF5, Fig. 2) and resulting in collapse (Fig. 9b). A crack (LF4; Fig. 2) at the front of sliding mass no. 1 caused the sliding mass to slide down and damage the highway (Fig. 9c). In addition, a 15-cm-wide tension crack (LF6;

Fig. 2) developed in the middle part of sliding mass no. 2, which also damaged the highway (Fig. 9d, the location is shown in D3 in Fig. 2).

Since the deformation of the Tanjiawan landslide began in 2014, the landslide has undergone obvious deformation during repeated rainfalls, and large-scale cracks (LF1–LF6; Fig. 2) have appeared in many places. Bounded by the convex of bedrock, the deformation above the boundary was relatively stable, the deformation of sliding mass no. 2, on the

Fig. 7 Deformation of the middle part of the Tanjiawan landslide owing to autumn rain in West China in 2017: **a** damage to houses caused by the deformation, **b** crack LF2 approximately 80 m long, **c** road damage caused by the cracks, **d** damage to the cement board due to the deformation of the sliding mass

Fig. 8 Landslide deformation caused by rainfall in 2018: **a** crack LF3 outside the highway in the middle of the landslide, **b** crack LF4 in the highway retaining wall at the front of the landslide

left side of the landslide, is relatively weak, whereas sliding mass no. 1, on the right side of the landslide, has undergone intense deformation in recent years. The structural characteristics observed in the survey indicate that sliding mass no. 1 is likely to be unstable under the effects of rainfall. However, there is no clear displacement response of the landslide during some rainfall events; therefore, it is necessary to analyse the deformation response of the Tanjiawan landslide using rainfall data and data from other types of landslide monitoring.

Multi-index monitoring results of the Tanjiawan landslide

Monitoring arrangement

Professional monitoring of the Tanjiawan landslide began in 2006. The initial monitoring setup included five GPS surface displacement monitoring points, two GPS datum points arranged at the bedrock outside the landslide, an LF1 crack monitoring point, and a rainfall monitoring point at the crack in the middle of the landslide. GPS data are collected manually, and the collection frequency is 1–2 times/month; therefore, the recorded displacement data are also 1–2 times/month. Crack and rainfall data are manually collected monthly, but daily data are recorded. Owing to the increasing deformation of the Tanjiawan landslide, the administration added new monitoring equipment in January 2020. The equipment includes 11 GNSS automatic surface displacement monitors, three deep displacement monitors, three groundwater level monitoring points, two soil moisture content monitors, and eight soil vibration and inclination monitors. All monitoring data are collected in real time and sent automatically. The layout of monitoring points is shown in Fig. 3.

Fig. 9 Intensified deformation throughout the landslide due to multiple rainfall events in June and July 2020: **a** break in the middle of the retaining wall due to sliding mass No. 1, **b** crack LF5 at the back of sliding mass No. 1, **c** intensified deformation of crack LF4, **d** damage of highway due to crack LF6 caused by sliding mass No. 1
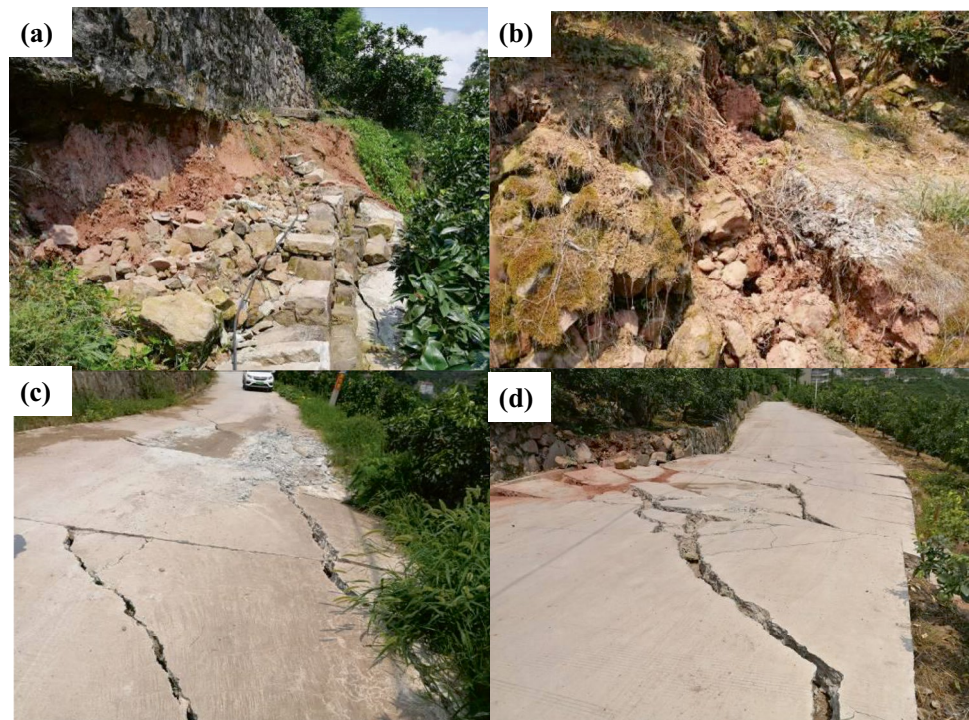
Response of groundwater level

Three groundwater level monitoring points, CX1, CX2, and CX3 from top to bottom, were identified in the borehole on the 2–2′ main profile of the Tanjiawan landslide in January 2020. A grit pipe was arranged at the bottom of the borehole, and a water level gauge was placed at a position 1 m from the bottom of the borehole. The groundwater level gauge is a pressure level gauge, in which the water level depth at the position of the measuring sensor is converted through the pressure difference; their locations and burial depths are shown in Fig. 3. The groundwater level and daily rainfall measured at these points were plotted in Fig. 10. Owing to the high elevation of the landslide front, the water level scheduling of the TGR does not affect the groundwater level of the Tanjiawan landslide. CX1 at the back edge of the landslide clearly responded to rainfall, and after three consecutive rainfall events, the groundwater level increased considerably and rapidly. There are two main reasons for this. One is the water catchment effect of the concave terrain where CX1 is located (Fig. 4b). In addition, it was speculated that multiple cracks were produced near the CX1 borehole and formed the dominant seepage channel. As there was no significant tension crack at the position of the CX2 and CX3 monitoring points and the permeability of the sliding mass soil was low, the groundwater levels at CX2 and CX3 did not change significantly for several months. However, after a large deformation in the middle and lower parts of the landslide in June 2020, the CX2 and CX3 monitoring points were also affected, and multiple cracks appeared. Subsequently, the water level at CX2 fluctuated by several meters during the rainfall. It is speculated that cracks near the CX2 borehole were generated owing to a previous deformation and formed the dominant seepage channel. After the severe

deformation in June, the groundwater level at CX3 increased sharply (by 15 m) and then remained essentially unchanged at an elevation of 204 m. An inspection of the site revealed that the groundwater level was close to the landslide surface, and because of severe deformation, the borehole at CX3 collapsed, resulting in instrument damage.

The changes in the groundwater level monitoring points were not uniform, and the analysis is related to the bedrock bulge and cracks in the landslide mass. To further determine the impact of rainfall on the groundwater level of the landslide, the finite element method software SEEP/W was used to simulate the changes in the groundwater level of the Tanjiawan landslide under rainfall conditions. The rainfall condition used was the actual rainfall from January to October 2020, and the calculation profile used geological profiles 2–2′. The calculated initial water level conditions used the results of the survey, as shown in Fig. 4b, and the unsaturated permeability function used the predicted value from the Fredlund-Xing equation based on the saturated permeability coefficient. The results of the groundwater level calculations are shown in Fig. 11. Multiple local saturation zones were formed by the rainfall in the landslide mass. Compared with the initial water level, the water level at the rear of the landslide changed significantly. In the numerical model, the same monitoring points as those for the actual groundwater levels were selected: CX1′, CX2′, and CX3′, as shown in Fig. 11a. The groundwater level results of the three numerical monitoring points CX1'–CX3' in the calculation period are plotted in Fig. 10. Compared with the actual groundwater level, the groundwater level changed at the CX1′ monitoring point which also changed, and the variation range reached 15 m; however, it was still significantly lower than the actual monitoring water level which changed by 30 m. However, owing to the special terrain of the CX2′ monitoring point, the simulation results were similar to the monitoring

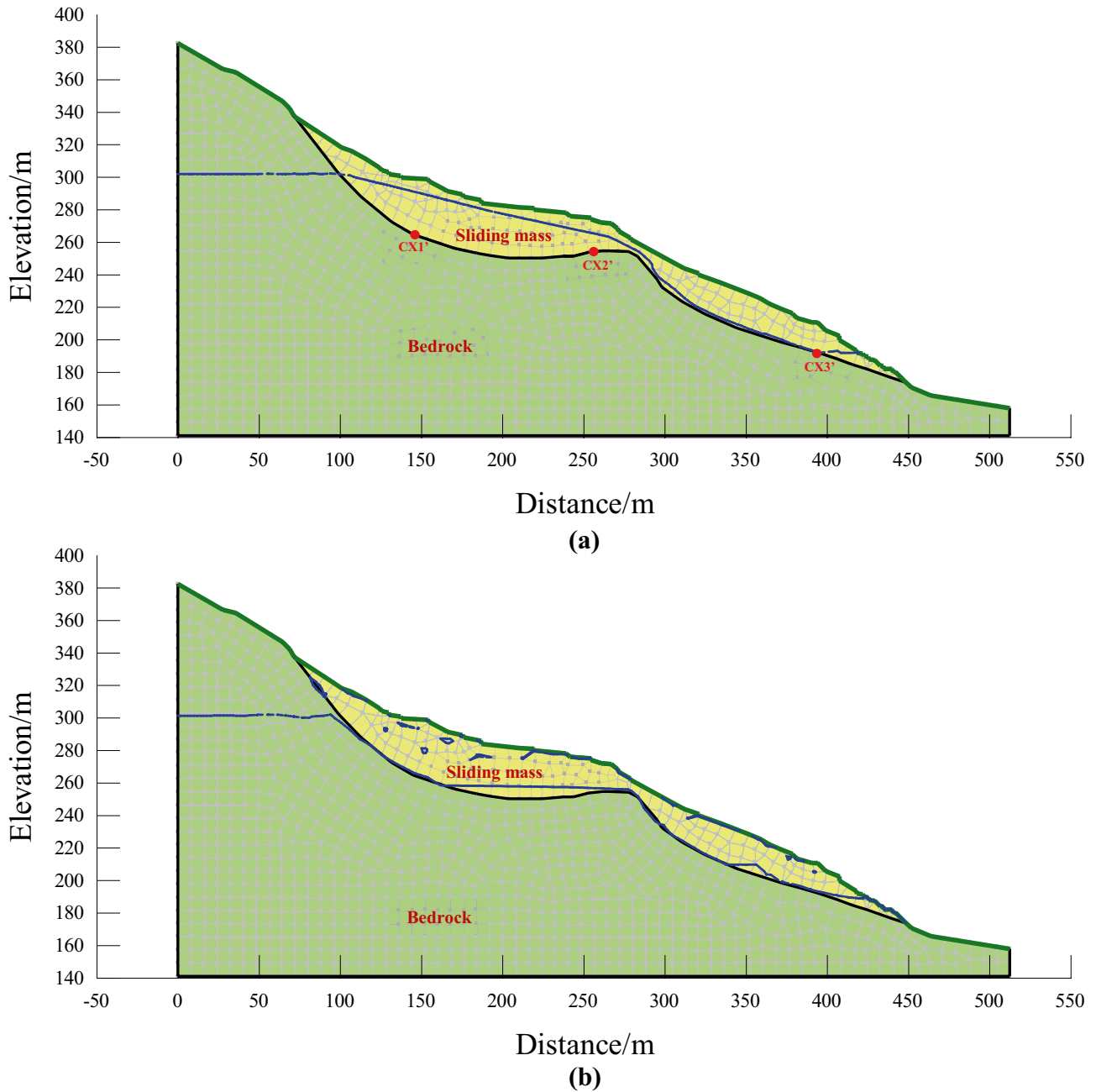Fig. 10 Relationship between groundwater level and rainfall in the Tanjiawan landslide
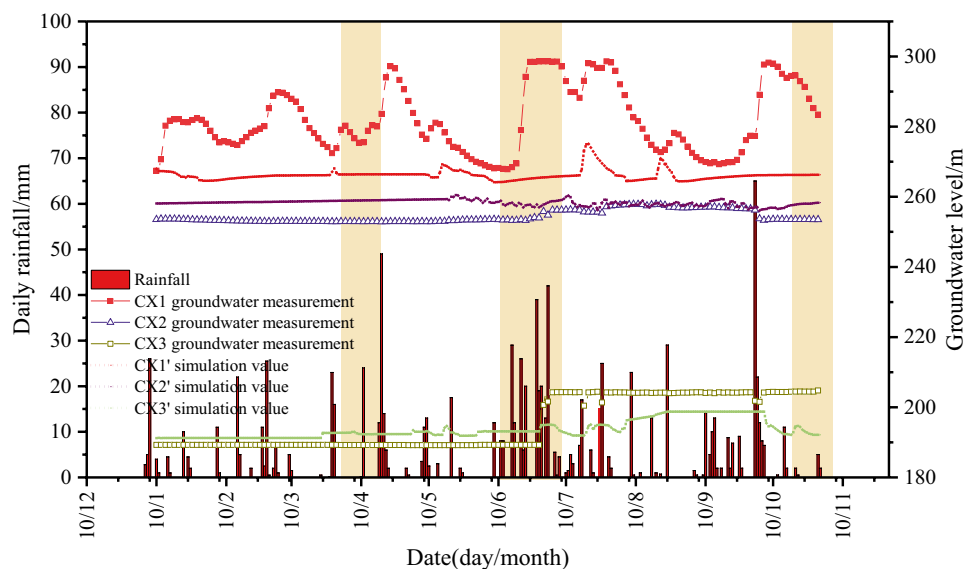
Fig. 11 Seepage simulation of the Tanjiawan landslide: **a** the groundwater level at day 1, **b** the groundwater level at day 305

results, and there was no significant difference. There was a large gap between the simulation results of CX3′ and the actual situation. Compared with the long-term unchanged monitoring results of the actual water level, the numerical simulation results showed significant fluctuations with the rainfall cycle. Obviously, the actual groundwater level monitoring at CX3 has technical problems. In general, the influence of bedrock shape on the change in the groundwater level of the Tanjiawan

landslide is relatively large, especially for the CX1′ monitoring point. SEEP/W has difficulty in simulating the effect of cracks, but the effect can be seen by comparing the simulation results with the actual results. The developed cracks were also the dominant seepage channel for surface water, causing rapid changes in the groundwater level. In short, the fluctuation in the groundwater level of the Tanjiawan landslide was the main hydrodynamic result caused by the recent large deformation.

Surface deformation in response to rainfall

GPS monitoring displacement

Since 2014, the Tanjiawan landslide has undergone obvious deformation during repeated rainfall events. To analyse the effects of rainfall on the deformation, GPS displacement data, monthly rainfall data, and reservoir water level data were plotted in Fig. 12. All GPS displacement data are resultant displacements in the horizontal and vertical directions. Owing to the limited wading range at the front of the landslide, fluctuations in the reservoir water level in the TGR do not affect the Tanjiawan landslide. Prior to 2014, the surface deformation of the landslide was dominated by slow creep deformation, and the largest cumulative displacement was at the ZG331 monitoring point in the middle of the landslide, which showed a displacement of only 88 mm. After 2014, multiple monitoring points showed step-like displacement curves. Specifically, in response to the rainfall of 31 August 2014, the displacement of ZG331 increased sharply to 153 mm; the surface deformation is shown in Fig. 7d. Other monitoring points still showed slow creep deformation. During the 2017 autumn rain in West China, the rainfall reached 286.8 mm in July and 409 mm in September and October. The five GPS monitoring points on the landslide all indicated severe deformation; that of ZG331 in the middle of the landslide was the most significant, with a sudden displacement increase of 265 mm. This rainfall event was also the first time that the entire landslide region underwent deformation. In response to the two heavy rainfall events in June 2018, strong deformation occurred at all the monitoring points on the landslide except at ZG332; again, the most obvious deformation occurred at ZG331 in the middle of the landslide. The cumulative displacement increased sharply, from 560 to 1388 mm, and the surface deformation was obvious (Fig. 8). Subsequently, the landslide can be divided into two deformation zones, the main deformation zone is the no. 1 sliding mass, and the secondary deformation zone is the no. 2 sliding mass. The rear part of the landslide is relatively stable. From 8 to 23 June 2020, several heavy rainfall events occurred in the landslide area, and 42 mm of rain fell on July 2. As a result, sliding mass no. 1 (except for the ZG332 monitoring point) exhibited the largest deformation to date and is still undergoing deformation. From May to October 2020, the displacements of ZG396 and ZG397 increased by nearly 1000 mm, that of ZG333 increased by approximately 2400 mm, and that of the central monitoring point ZG331 increased by approximately 2700 mm. Sliding mass no. 1 showed an overall sliding trend.

Automatic crack meter monitoring displacement

The GPS displacement data reported above are usually obtained once or twice a month, and the analysis of the
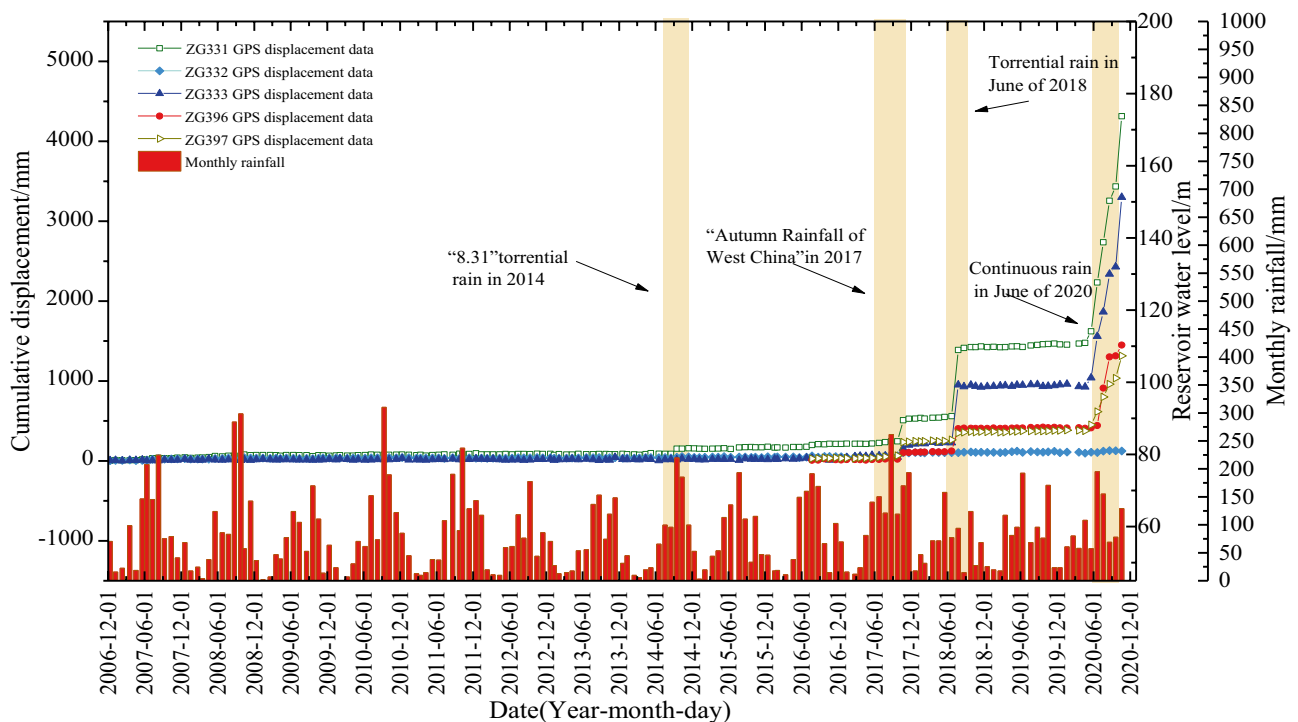

Fig. 12 Response relationship between GPS displacement and rainfall in the Tanjiawan landslide

relationship between monthly rainfall and GPS displacement cannot accurately indicate the real deformation process of the landslide. Therefore, in June 2016, an SRL-16 surface crack metre manufactured by Japan's Fantian Motor was used to monitor surface cracks (details of the instrument in Wang et al. 2021a, b). The monitor was installed at the crack near the GPS monitoring point ZG331, which has shown the largest deformation, for the automatic daily recording of the crack displacement data. Rainfall has been monitored in the landslide area since April 2017. The plot of the relationship between the measured dynamic crack deformation and daily rainfall (Fig. 13) shows that ACM1 is under continuous tension. Figure 13 shows that the 2017 autumn rain in West China strongly affected the displacement of ACM1, and the cumulative displacement reached 76 mm. The resulting deformation occurred during the continuous rainfall event, under the heavy rainfall of 65 mm on 2 October, and then the deformation continued to increase. The figure shows a steep increase in the displacement of ACM1 induced by heavy rainfall on 5 July 2018. Before the landslide deformation occurred, the daily rainfall in the landslide area was 121.6 mm on June 18 and 27.4 mm on June 30; these rainfall events were the main causes of the deformation. In June 2020, from Fig. 13, we can see a steep increase in the displacement of ACM1 caused by continuous rainfall for several days. Rainfall occurred on 12 of 25 days before the deformation occurred, and the average daily rainfall was 21.2 mm; the rain dramatically increased the displacement by as much as 720 mm. Then, the instrument was damaged and lost its monitoring function.

GNSS monitoring displacement and soil moisture content

The GNSS displacement monitoring instruments that were installed in January 2020 have the advantage of transmitting the information on landslide deformation in real time. Four points with obvious deformation (G3, G7, G8, and G9) were selected to plot the relationship between displacement and daily rainfall (Fig. 14). The displacements at the other monitoring points were the same as those at G5 and did not show obvious deformation. Sliding mass no. 1 clearly showed the most extensive deformation, and all of the monitoring points exhibited a large displacement. The deformation of the back part in no. 2 sliding mass was more obvious. The deformation of the Tanjiawan landslide in 2020 could be divided into three stages: first stage — continuous deformation in late June 2020, second stage — accelerated deformation in late July 2020, and third stage — strong deformation on 3 October 2020. A comparison of the deformation data showed that the deformation in the first two stages had a relatively clear lag with respect to rainfall. The third stage was dominated by the deformation of sliding mass no. 1 that was caused by heavy rainfall (65 mm) on the day before the deformation.

To further compare the effects of rainfall on the three deformation processes of the landslide, the displacement of G8 (which showed clear deformation) and the soil moisture content at T2, near G8, with rainfall data were plotted as shown in Fig. 15. The soil moisture content sensor was located at a depth of 0.5 m. Prior to April 2020, the rainfall was generally scant, and the soil moisture content was below

Fig. 13 Automatic crack displacement metre data from ACM1 for recent unusual rainfall events
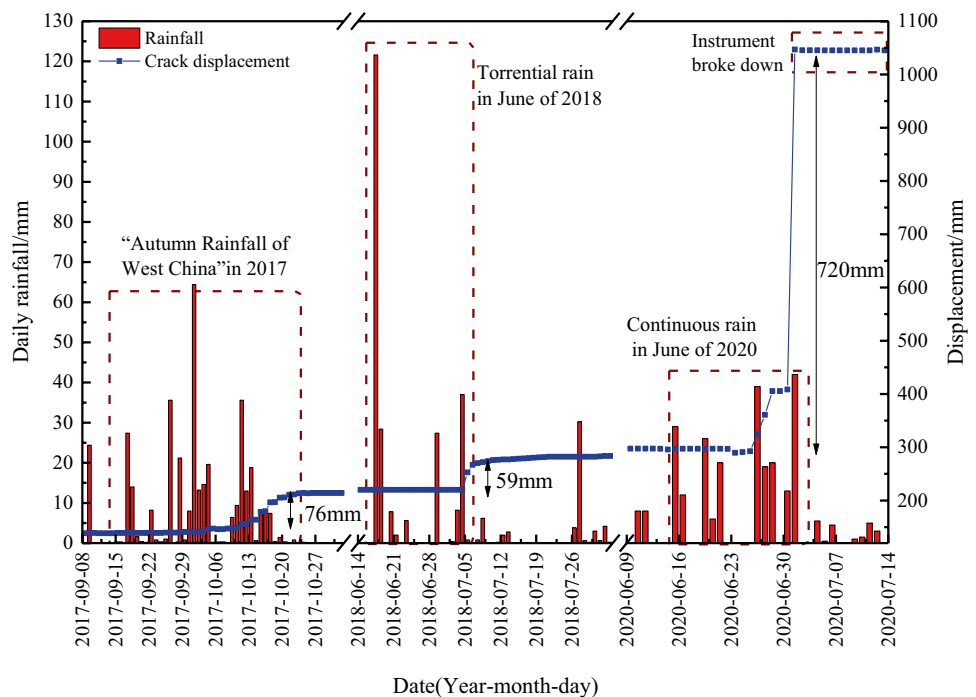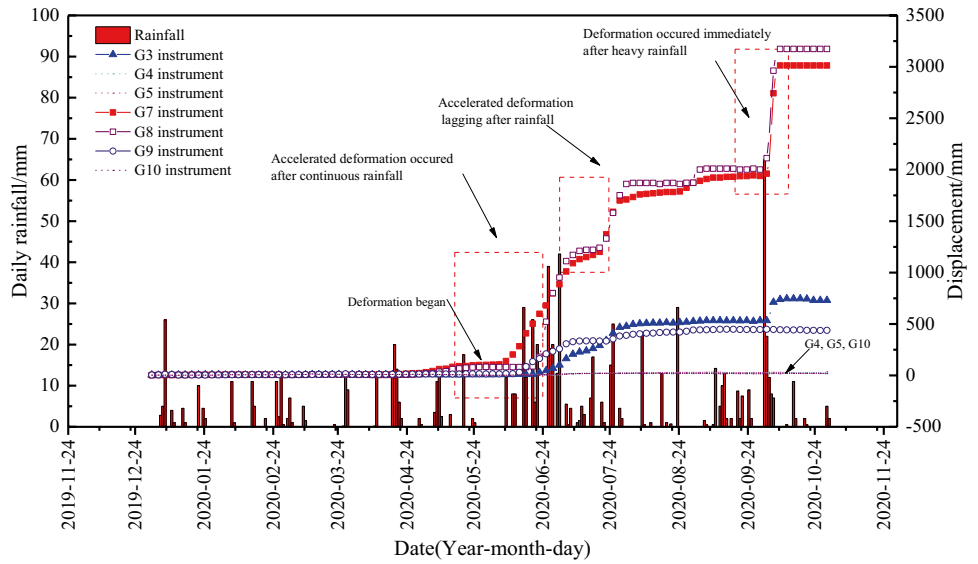
Fig. 14 Response of GNSS monitoring displacement instruments to the rainfall in 2020

10% for an extended period. Several rainfall events in April increased the soil moisture content, and the displacement of G8 also began to increase slowly. During the continuous rainfall in June, the soil moisture content increased rapidly, with a corresponding increase in displacement. In response to the rainfall on 2 October (65 mm), the moisture content increased sharply, nearly saturating the soil, and a significant response in displacement was also observed. Continuous and heavy rainfalls will clearly increase the moisture content of landslide soil; in particular, heavy rainfall may cause the

surface soil to enter the transient saturation zone, eventually resulting in severe deformation of the surface.

Deep displacement and dip angle variation

Three deep displacement monitoring holes were established on the 2–2′ main profile of the Tanjiawan landslide in January 2020 (Fig. 3). The monitoring equipment included an inclinometer with one side embedded in the bedrock at least 1–2 m.
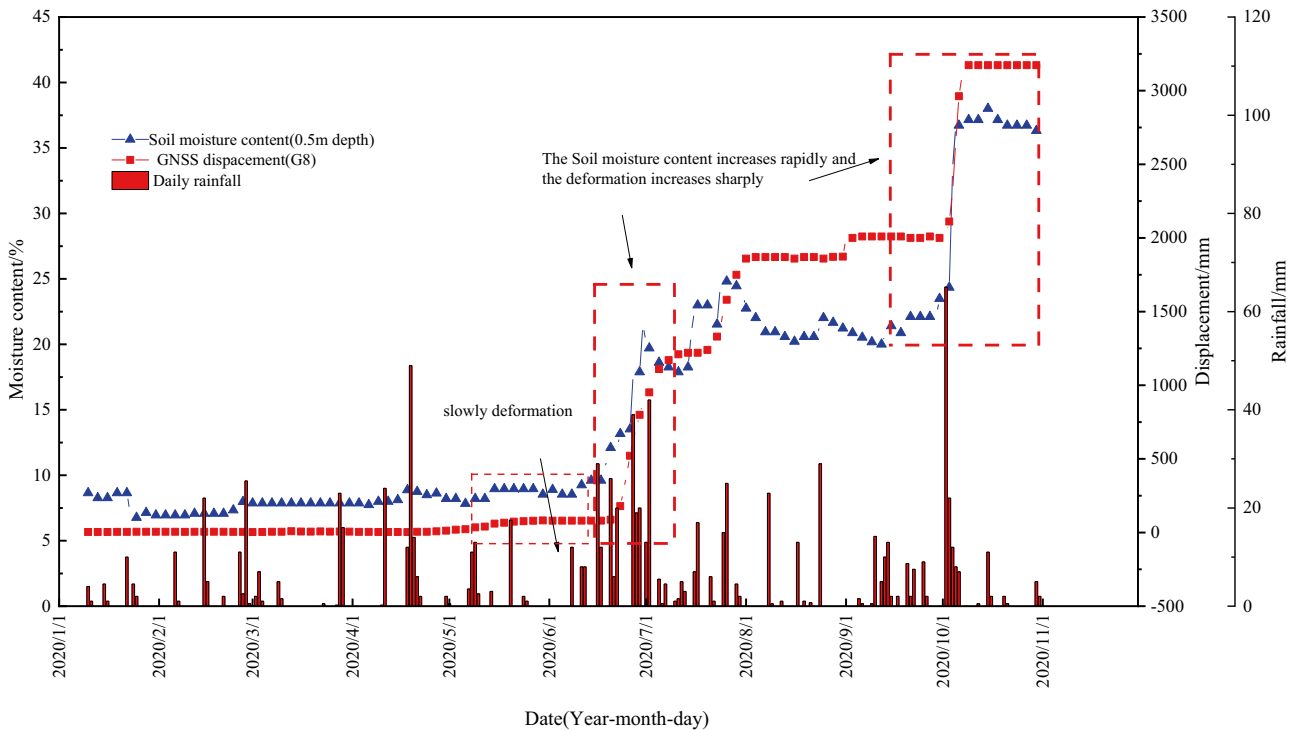

Fig. 15 Relationship among rainfall, soil moisture content and displacement

Among the monitoring points, CX2 and CX3 showed obvious deformation (Fig. 16), the sliding surface depths of CX2 and CX3 monitoring points are 29.5 m and 18.1 m, respectively. The deep deformation observed at CX2 appeared mainly at 4–7 m, and the overall deformation appeared at a depth of 15–27 m in June. CX3 showed deformation at a shallow level of 1–4 m. Overall, the 2–2′ main profile showed no deep sliding, and no significant deformation of the contact between the sliding surface and bedrock was observed in the survey. However, sliding at the shallow depths was more prominent.

Microcore pile is a new type of geological hazard monitoring and warning system that can monitor the vibration acceleration, inclination, and vibration curve, perform sudden displacement calculation, measure other indicators, and conduct real-time warning and data transmission. In particular, it can record the slight vibration that occurs before landslide sliding, which provides a good early warning. Eight microcore piles were placed at the locations shown in Fig. 3 in 2020. The monitoring data of WX3 and WX4 on the main profile 2–2′ and the adjacent GNSS monitoring points G7 and G8 were plotted as shown in Fig. 17. The microcore pile vibrated before many strong deformation events, and the change in soil inclination recorded by the pile was consistent with the deformation response of the landslide surface. In particular, the inclination recorded by the WX4 monitoring point increased by approximately 90°,

and it was found that this outburst was severely deformed during surface surveys.

Discussion

The Tanjiawan landslide began to show significant deformation in 2014. Currently, the back of the landslide is relatively stable, and intense deformation is occurring in the middle and at the front of the landslide. According to the deformation characteristics, the landslide can be divided into sliding masses no. 1 and no. 2, where no. 1 is the active deformation area. The investigation results revealed that the bedrock in the middle of the landslide protrudes outward, and this natural feature has prevented sliding, and is also the dividing line of the landslide deformation area. The deformation above the boundary was relatively stable, the deformation below the boundary was relatively severe.

An analysis of the monitoring results in "Multi-index monitoring results of the Tanjiawan landslide" revealed that rainfall was the most important factor in landslide deformation. Prior to 2014, neither long rainfall events nor short rainstorms triggered obvious deformations of the Tanjiawan landslide, the main reason being the weak permeability of the sliding body, which made it extremely difficult for rainfall to deeply penetrate the sliding mass. Several cracks appeared in the landslide body after 2014; in particular, fractures that

Fig. 16 Deep displacement curve (January to October 2020) at **a** CX2 and **b** CX3
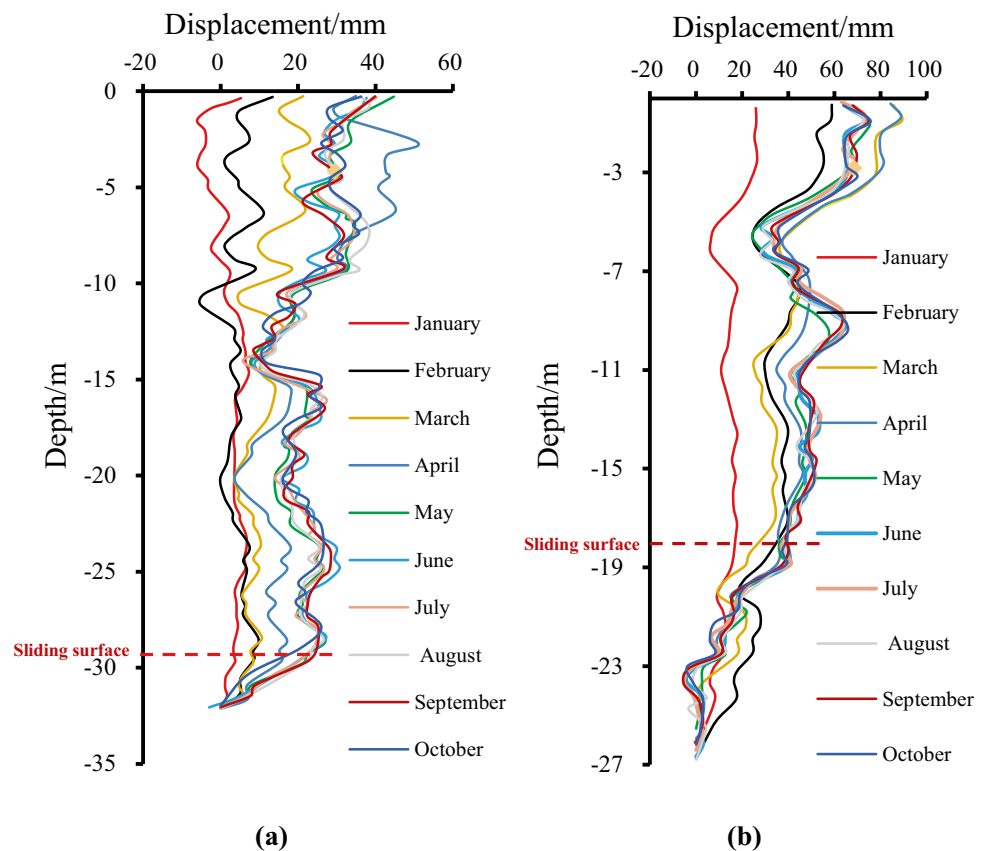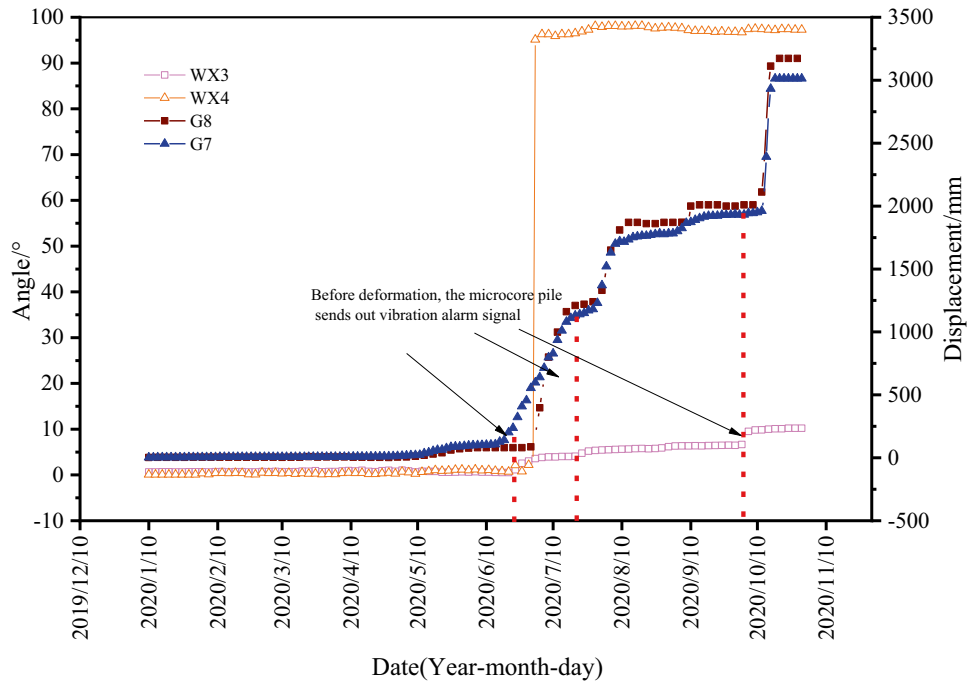
(a)   **(b)**

Fig. 17 Microcore pile monitoring data from WX3 and WX4 on the main profile 2–2′ and adjacent GNSS monitoring points G7 and G8

developed in 2017 resulted in the formation of dominant channels for rainfall infiltration. The heavy rainfall of June 2018 caused further deformation. GPS displacement monitoring data showed that the deformation of the Tanjiawan landslide with time showed a typical step shape. The deformation intensified even more in 2020, and the number of cracks and dominant seepage channels for rainfall infiltration in the sliding mass increased, further facilitating rainfall infiltration into the landslide. Specifically, the groundwater level at CX2 and CX3 began to exhibit a significant response to rainfall (Fig. 9). The effect of the groundwater level fluctuation on the landslide deformation was also explored. The groundwater level data for the 2–2′ profile at CX2 and CX3

and the data from the adjacent displacement monitoring point G8 from 10 June to 7 July 2020 are shown in Fig. 18. The landslide deformation at CX2, in the middle of the landslide, clearly responded to the change in water level, and the landslide began to deform after the underground water level increased. The groundwater level at CX3 (located at the front of the landslide) increased steeply after the severe deformation of the landslide and was found to be only 4 m below the surface after the event. The groundwater level at CX3 remained stable. The increase in cracks in the landslide allowed rainwater infiltration, and the subsequent increase in the groundwater level produced hydrodynamic pressure that caused the landslide to deform dramatically. The

Fig. 18 Relationship between groundwater level fluctuation and landslide deformation
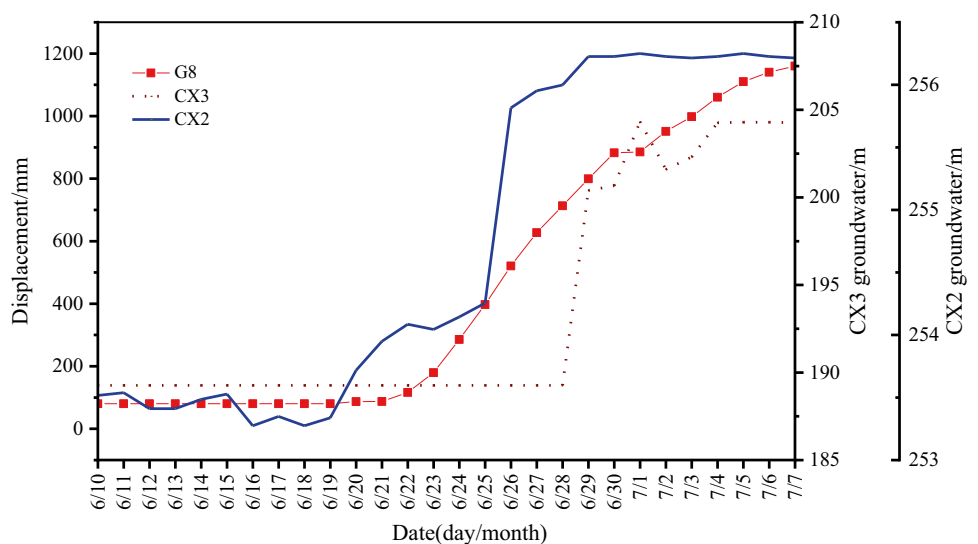
hydrodynamic pressure itself was the result of both continuous light rain and short-term rainstorms, and thus both types of rainfall events affected the landslide.

Monitoring is one of the important components of landslide early warning systems (LEWS), and the effective use of monitoring results was the main research purpose of this study. Note that the abrupt increase in soil moisture content occurred before the strong deformation of the landslide; hence, this phenomenon can be used as an early warning of landslide instability. However, in general, it is difficult to accurately determine the necessary warning time by directly observing the change in soil moisture content. As shown in Fig. 15, we can find that the rate of change in moisture content has a direct impact on the magnitude of the displacement. The relationship between the displacement change rate and soil moisture change rate is shown in Fig. 19. When the landslide undergoes a large deformation, the change rate in the soil moisture content increases significantly. For example, the displacement change rate on September 1 reached 127 mm/day, which corresponded to the moisture content change rate on August 25 at 1.18%/day. The largest deformation occurred on October 2, 2020, and the moisture content change rate 2 days earlier reached 8.96%/day. When the rate of change in water content was lower than 1%/day, generally no major deformation occurred. Obviously, the change rate in soil moisture content can be used as an important early warning criterion for landslide deformation. Therefore, for LEWSs, we can calculate the change in

soil moisture content every day compared to the previous day, and through long-term monitoring, obtain a threshold moisture content change rate, such as 1%, as the landslide deformation warning value.

As an important part of an LEWS, multi-index monitoring methods, such as surface deformation, deep displacement, groundwater, and soil moisture content monitoring, have been conducted on the Tanjiawan landslide. In the monitoring of surface deformation, three methods including GPS, surface cracks, and GNSS were used. Among these methods, GNSS monitoring technology was applied for the first time to a landslide in the TGRA. This technology can automatically send displacement data in real time, overcoming the past inconvenience of manual collection and insufficient data timeliness. Similarly, soil moisture content as a monitoring parameter was also applied for the first time to landslides in the TGRA. The response relationship with GNSS shows that the change rate in soil moisture content can be used as an early warning indicator of landslide deformation. However, the monitoring of pore water pressure and matric suction is not included in the monitoring of hydrological indicators of landslides. Therefore, it is difficult to obtain suitable early warning indicators for the deformation and failure of landslides under unsaturated conditions. Thus, establishing the response relationship with displacement based on a variety of hydrological monitoring methods will be an effective method for early warning of rainfall-type landslides in the future.

Fig. 19 Relationship between the displacement change rate and soil moisture change rate
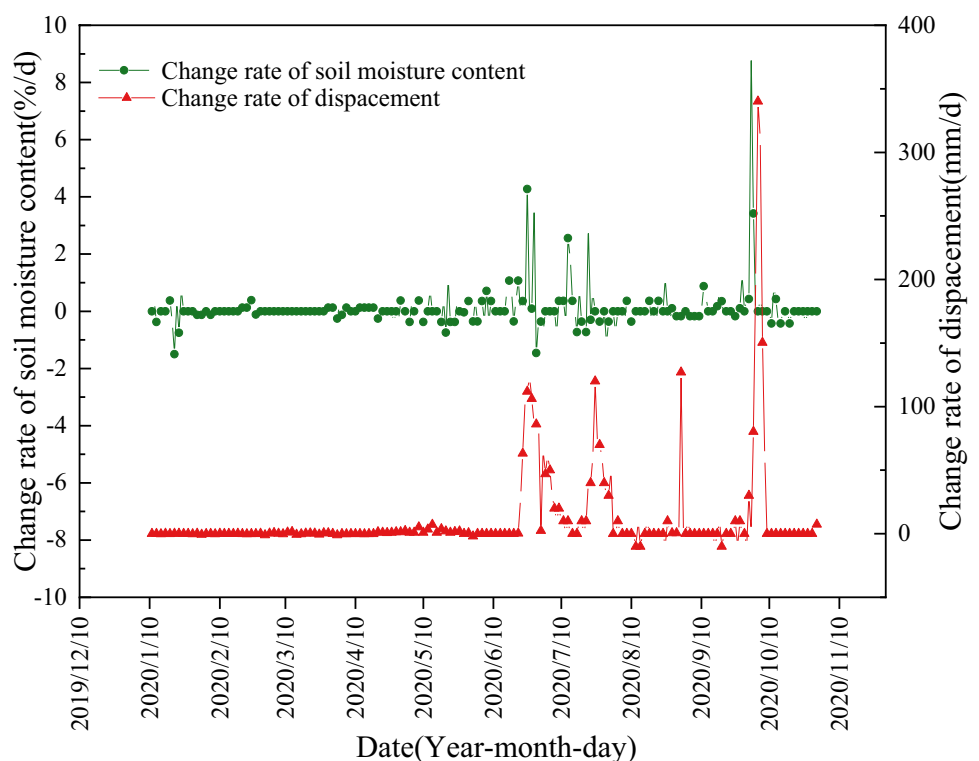
Conclusion

First, the deformation of the Tanjiawan landslide is a function of various geological conditions, including stratigraphic lithology and slope structure. In addition, rainfall is another important factor affecting deformation. Based on the surface deformation characteristics, surface displacement monitoring data, and slope structure revealed by the survey, the Tanjiawan landslide can be divided into two deformation zones, no. 1 and no. 2, the former being more active. At present, the deep displacement behaviour reveals that the Tanjiawan landslide is dominated by surface deformation, and the overall sliding process of the landslide is discontinuous. However, further development of the cracks may cause sliding mass no. 1 to slip.

The displacement and deformation curves of the Tanjiawan landslide show step-like features. Prior to 2014, the deformation was mainly peristaltic owing to the weak permeability of the sliding mass soil. Subsequently, cracks developed gradually in the Tanjiawan landslide. Since August 2014, owing to continuous rainfall or short-term rainstorms, the surface water has formed dominant seepage along the cracks, and the groundwater level in the middle and rear parts of the landslide has risen significantly owing to the influence of the bedrock morphology. The resulting dynamic water pressure has caused the displacement to increase sharply, which is the main reason for the steps in the displacement curve.

In conclusion, the deformation rate and frequency of the Tanjiawan landslide are increasing with time, and the landslide cracks are widely distributed, especially those in sliding mass no. 1. If the sliding surfaces connect, sliding mass no. 1 is likely to be unstable overall. Therefore, further studies on a landslide warning system based on various monitoring methods are imperative. The seismic data recorded by microcore piles and change rate in soil moisture content after rainfalls can currently be used for early warnings of landslide instability.

Declarations

Conflict of interest The authors declare no competing interests.

References

Alonso E, Gens A, Lloret A, Delahaye C (1995) Effect of rain infiltration on the stability of slopes. In: Proceedings of the first international conference on unsaturated soils, UNSAT'95, Paris, France, vol 1, pp 241–249

Baum RL, Godt JW (2010) Early warning of rainfall-induced shallow landslides and debris flows in the USA. Landslides 7:259–272. https://doi.org/10.1007/s10346-009-0177-0

Bordoni M, Meisina C, Valentino R et al (2015) Hydrological factors affecting rainfall-induced shallow landslides: from the field monitoring to a simplified slope stability analysis. Eng Geol 193:19–37. https://doi.org/10.1016/j.enggeo.2015.04.006

Bordoni M, Bittelli M, Valentino R et al (2021) Observations on soil-atmosphere interactions after long-term monitoring at two sample sites subjected to shallow landslides. Bull Eng Geol Environ 80:7467–7491. https://doi.org/10.1007/s10064-021-02334-y

Damiano E (2019) Effects of layering on triggering mechanisms of rainfall-induced landslides in unsaturated pyroclastic granular soils. Can Geotech J 56(9):1278–1290. https://doi.org/10.1139/cgj-2018-0040

Ding JX, Yang ZF, Shang YJ et al (2006) A new method for spatio-temporal prediction of rainfall- induced landslide. Science in China 4:421–430. https://doi.org/10.1007/s11430-006-0421-6

Du J, Yin K, Lacasse S (2013) Displacement prediction in colluvial landslides, Three Gorges Reservoir. China Landslides 10(2):203–218. https://doi.org/10.1007/s10346-012-0326-8

Dikshit A, Satyam N (2019) Probabilistic rainfall thresholds in Chibo, India: estimation and validation using monitoring system. J Mt Sci 16:870–883. https://doi.org/10.1007/s11629-018-5189-6

Godt JW, Baum RL, Lu N (2009) Landsliding in partially saturated materials. Geophys Res Lett 36:L02403. https://doi.org/10.1029/2008GL035996

Hojat A, Arosio D, Ivanov VI et al (2019) Geoelectrical characterization and monitoring of slopes on a rainfall-triggered landslide simulator. J Appl Geophys. https://doi.org/10.1016/j.jappgeo.2019.103844

Huang D, Luo SL, Zhong Z et al (2020a) Analysis and modeling of the combined effects of hydrological factors on a reservoir bank slope in the Three Gorges Reservoir area. China Engineering Geology 279. https://doi.org/10.1016/j.enggeo.2020.105858

Huang XH, Guo F, Deng ML et al (2020b) Understanding the deformation mechanism and threshold reservoir level of the floating weight-reducing landslide in the Three Gorges Reservoir area, China. Landslides 17:2879–2894. https://doi.org/10.1007/s10346-020-01435-1

Liu JQ, Tang HM, Li Q et al (2018) Multi-sensor fusion of data for monitoring of Huangtupo landslide in the three Gorges Reservoir (China). Geomat Nat Haz Risk 9(1):881–891. https://doi.org/10.1080/19475705.2018.1478892

Lora M, Camporese M, Troch PA, Salandin P (2016) Rainfall-triggered shallow landslides: infiltration dynamics in a physical hillslope model. Hydrol Process 30(18):3239–3251. https://doi.org/10.1002/hyp.10829

Mirus BB, Becker RE, Baum RL et al (2018) Integrating real-time subsurface hydrologic monitoring with empirical rainfall thresholds to improve landslide early warning. Landslides 15:1909–1919. https://doi.org/10.1007/s10346-018-0995-z

Rahardjo H, Lim TT, Leong EC et al (2005) Response of a residual soil slope to rainfall. Can Geotech J 42:340–351. https://doi.org/10.1139/t04-101

SL237–1999 (1999) Specification of soil test. Ministry of Water Resources, China (in Chinese)

Song K, Wang F, Zuo Q et al (2020) Successful disaster management of the July 2020 Shaziba landslide triggered by heavy rainfall in Mazhe Village, Enshi City, Hubei Province. China Landslides (prepublish). https://doi.org/10.1007/s10346-020-01565-6

Sun P, Wang G, Wu LZ et al (2019) Physical model experiments for shallow failure in rainfall-triggered Loess slope, Northwest China.

Bull Eng Geol Env 78(6):4363–4382. https://doi.org/10.1007/s10064-018-1420-5

Tang H, Wasowski J, Juang CH (2019) Geohazards in the Three Gorges Reservoir area, China – lessons learned from decades of research. Eng Geol 261. https://doi.org/10.1016/j.enggeo.2019.105267

Tang M, Xu Q, Huang R (2015) Site monitoring of suction and temporary pore water pressure in an ancient landslide in the Three Gorges Reservoir area. China Environmental Earth Sciences 73(9):5601–5609. https://doi.org/10.1007/s12665-014-3814-4

Wang FW, Zhang YM, Huo ZT et al (2008) Movement of the Shuping landslide in the first four years after the initial impoundment of the Three Gorges Dam Reservoir. China Landslides 5(3):321–329. https://doi.org/10.1007/s10346-008-0128-1

Wang JE, Xiang W, Lu N (2014) Landsliding triggered by reservoir operation: a general conceptual model with a case study at Three Gorges Reservoir. Acta Geotech 9(5):771–788. https://doi.org/10.1007/s11440-014-0315-2

Wang L, Li G, Chen Y et al (2021a) Field model test on the disaster mechanism of artificial cut slope rainfall in Southern Jiangxi.

Rock Soil Mech 42(3): 846–854. https://doi.org/10.16285/j.rsm.2020.1129

Wang SM, Pan YC, Wang L et al (2021b) Deformation characteristics, mechanisms, and influencing factors of hydrodynamic pressure landslides in the Three Gorges Reservoir: a case study and model test study. Bull Eng Geol Environ 80(4):3513–3533. https://doi.org/10.1007/s10064-021-02120-w

Wu Q, Tang H, Ma X et al (2019) Identification of movement characteristics and causal factors of the Shuping landslide based on monitored displacements. Bull Eng Geol Env 78(3):2093–2106. https://doi.org/10.1007/s10064-018-1237-2

Wu T, Jia J, Jiang N et al (2020) Model test of deformation evolution and multi factor prediction of anchorage slope stability under rainfall condition. J Earth Sci 31:1109–1120. https://doi.org/10.1007/s12583-020-1343-5

Zhou C, Yin K, Cao Y et al (2016) Application of time series analysis and PSO–SVM model in predicting the Bazimen landslide in the Three Gorges Reservoir, China. Eng Geol 204:108–120. https://doi.org/10.1016/j.enggeo.2016.02.009